Supplementary Materials

Contents:

1. Thermal analyses
Fig. S1.1 TG/DSC study of cyclohexylammonium *β*-octamolybdate dihydrate (**1**).
Fig. S1.2 TG/DSC study of cyclohexylammonium trimolybdate hydrate (**2**).
Fig. S1.3 TG/DSC study of anilinium trimolybdate dihydrate (**5**).

2. Thermal stability studies by XRPD
Fig. S2.1 XRPD/temp. study of cyclohexylammonium *β*-octamolybdate dihydrate (**1**).
Fig. S2.2 XRPD/temp study of cyclohexylammonium trimolybdate hydrate (**2**).
Fig. S2.3 XRPD/temp study of anilinium trimolybdate dihydrate (**5**).

3. Crystallographic data:
Fig. S3.1 Cyclohexylammonium trimolybdate hydrate—Rietveld refinement plots (**2**).
Fig. S3.2 Anilinium trimolybdate dihydrate—Rietveld refinement plots (**5**).
Table S3.1 Cyclohexylammonium *β*-octamolybdate dihydrate—interatomic distances (**1**).
Table S3.2 Cyclohexylammonium trimolybdate hydrate—interatomic distances (2).
Table S3.3 Anilinium trimolybdate dihydrate—interatomic distances (**5**).

4. Kinetic modelling and catalytic results at 55 °C and catalyst stability:
Fig. S4.1 Experimental data (markers) and calculated kinetic curves (lines) for Cy (o) and epoxide CyO (Δ) concentration, based on the model A, for catalyst **1** (a), **2** (b), **3** (c), **4** (d), **5** (e) and **6** (f), at 70 °C.
Fig. S4.2 Experimental data (markers) and calculated kinetic curves (lines) for Cy (o) and epoxide CyO (Δ) concentration, based on the model B, for catalyst **1** (a), **2** (b), **3** (c), **4** (d), **5** (e) and **6** (f), at 70 °C.
Fig. S4.3 Experimental data (markers) and calculated kinetic curves (lines) for Cy (o) and epoxide CyO (Δ) concentration, based on the model C, for catalyst 1 **1** (a), **2** (b), **3** (c), **4** (d), **5** (e) and **6** (f), at 70 °C.
Fig. S4.4 Experimental data (markers) and calculated kinetic curves (lines) for Ole (o) and OleOx (Δ) concentration for catalyst **1** (a), **2** (b), **3** (c), **4** (d), **5** (e) and **6** (f), at 70 °C.
Fig. S4.5 Experimental data (markers) and calculated kinetic curves (lines) for Lin (o), LinOx (Δ), LimDiOx (×) and LinFur (+) concentration for catalyst **1** (a), **2** (b), **3** (c), **4** (d), **5** (e) and **6** (f), at 70 °C.
Fig. S4.6 *cis*-Cyclooctene epoxidation with TBHP, in the presence of the IPOM catalysts **3**–**5**, at 55 °C. Epoxide selectivity was always 100 %.
Table S4.3 Comparison of the catalytic results for **3**–**5** to literature data for IPOM compounds possessing anilinium derivatives as organic components, tested for the Cy/TBHP reaction, at 55 °C.
Fig. S4.7 Typical epoxidation catalytic test (with catalyst) (○) and contact tests (×) for *cis*-cyclooctene epoxidation with TBHP, in the presence of the IPOM catalysts **1**-**6**, at 70 °C.
Fig. S4.8 ATR FT-IR spectra (a) and powder XRD patterns (b) of the original and recovered solids **1**, **2**, **3** and **5**. The experimental details of the characterisation techniques are indicated.

Fig. S4.9 Kinetic constants as a function of density Dx (left) and n(oxo)/Mo ratio (right), for the Cy6N (a, b) and Anil (c, d) families of IPOM catalysts with different substrates (Cy (circles), Ole (squares) and Lin (triangles); the dotted lines are trendlines).
Fig. S4.10 Examples of chromatograms for Cy, Ole and Lin reactions.

1. Thermal analyses

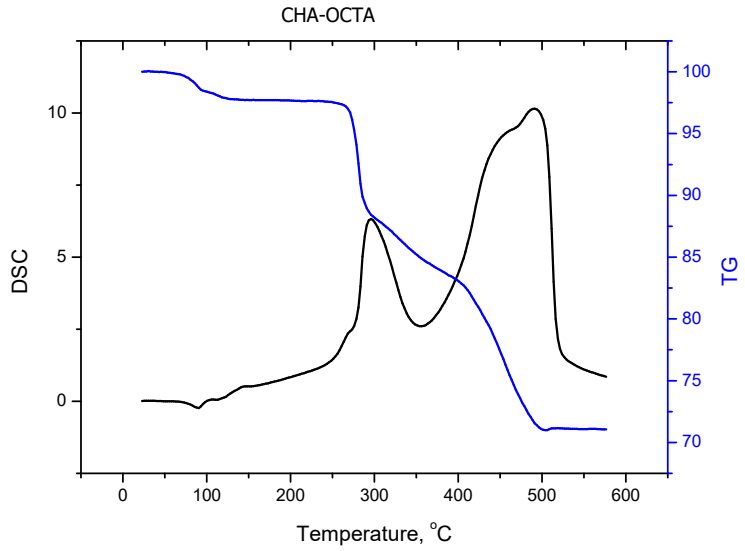

Fig. S1.1. TG/DSC study of cyclohexylammonium *β*-octamolybdate dihydrate (**1**).

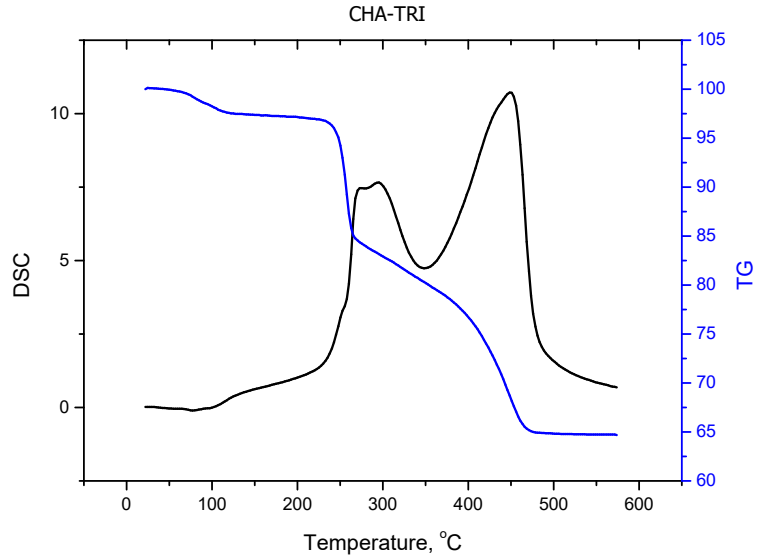

Fig. S1.2. TG/DSC study of cyclohexylammonium trimolybdate hydrate (**2**)

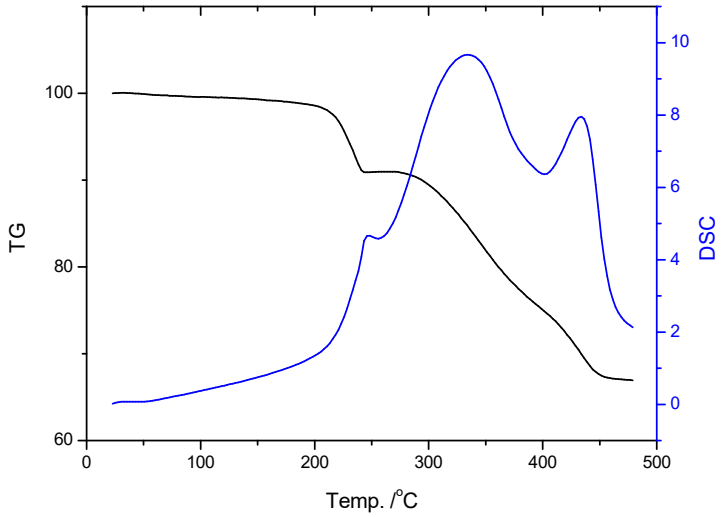

Fig. S1.3. TG/DSC study of anilinium trimolybdate dihydrate (**5**).

2. Thermal stability studies by XRPD

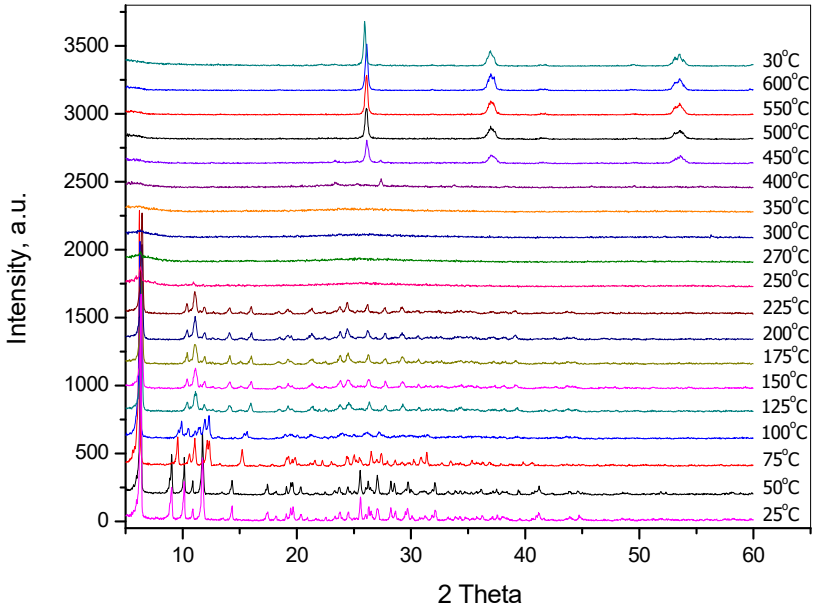

Fig. S2.1. XRPD/temp study of cyclohexylammonium *β*-octamolybdate dihydrate (**1**).

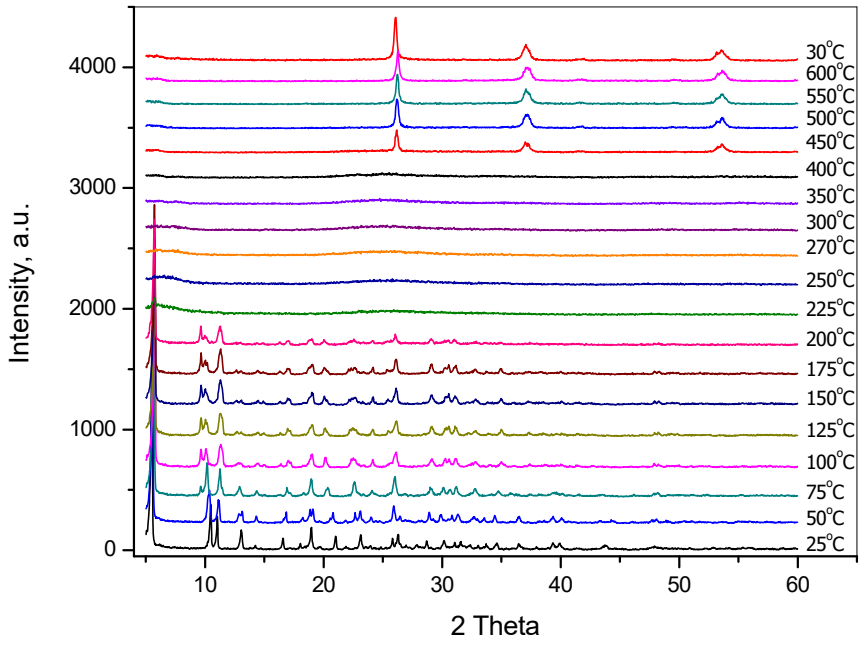

Fig. S2.2. XRPD/temp study of cyclohexylammonium trimolybdate hydrate (**2**).

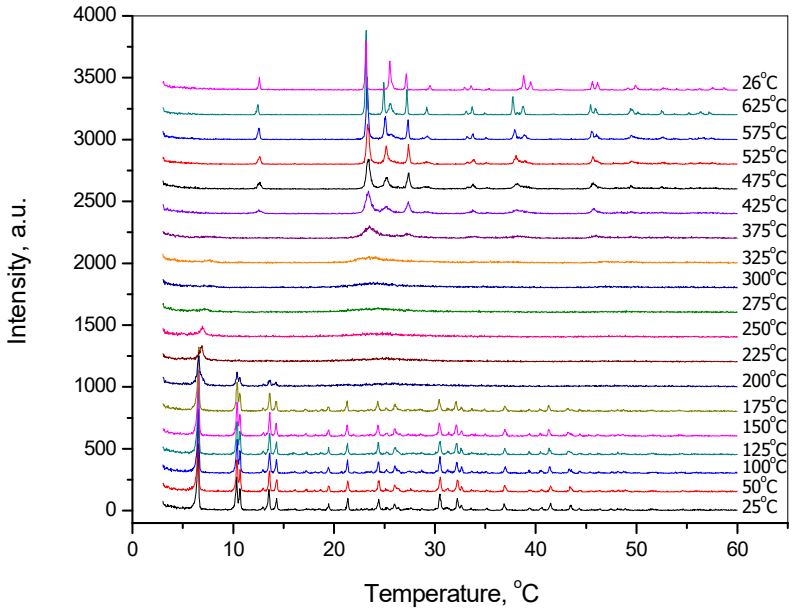

Fig. S2.3. XRPD/temp study of anilinium trimolybdate dihydrate (**5**)

3. Crystallographic data

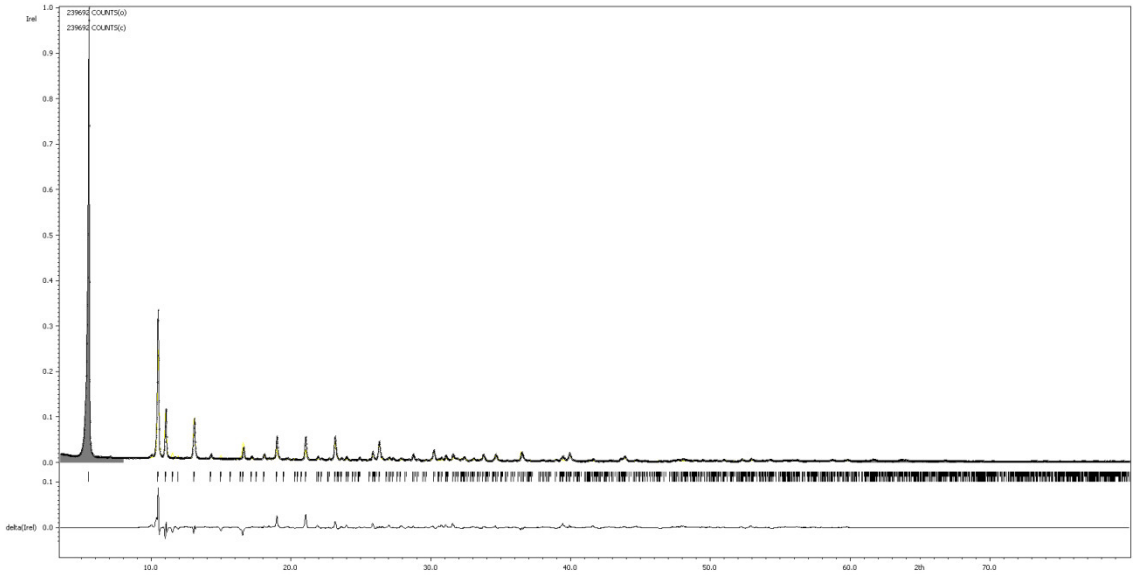

Fig. S3.1 Cyclohexylammonium trimolybdate hydrate—Rietveld refinement plots (**2**). Due to strong asymmetry, the first peak at 5s was excluded from calculations.

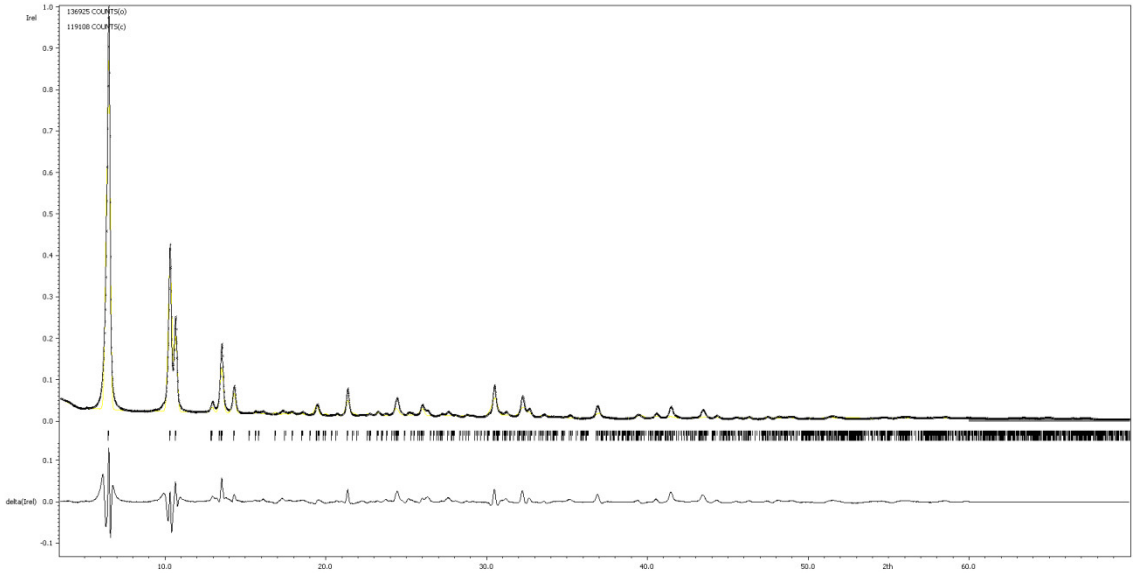

Fig. S3.2. Anilinium trimolybdate dihydrate—Rietveld refinement plots (**5**).

Table S3.1. Cyclohexylammonium β-octamolybdate dihydrate—interatomic distances (**1**).

Mo – O (symm. code)	Distance (esd) Å	Mo – O (symm. code)	Distance (esd) Å
Mo1-O1	1.9140(19)	Mo3-O1	1.9341(18)
Mo1-O2	1.707(2)	Mo3-O3	1.696(2)
Mo1-O9	1.700(2)	Mo3-O4	1.717(3)
Mo1-O11	2.323(2)	Mo3-O5^i^	1.9193(15)
Mo1-O12	1.9965(17)	Mo3-O10	2.300(2)
Mo1-O13	2.3278(16)	Mo3-O13	2.4813(18)

Mo2-O8	1.709(3)	Mo4-O5	1.8845(18)
Mo2-O10^i^	1.7559(18)	Mo4-O6	1.704(3)
Mo2-O11^i^	1.9474(16)	Mo4-O7	1.7173(16)
Mo2-O12	1.9281(17)	Mo4-O11	2.0168(18)
Mo2-O13	2.1465(19)	Mo4-O12	2.330(2)
Mo2-O13^i^	2.380(2)	Mo4-O13^i^	2.3047(16)
(i) -x+2,-y-1,-z+1			
N2-C21	1.508(5)	C25-C26	1.526(5)
N4-C41	1.496(4)	C41-C42	1.515(5)
C21-C22	1.523(5)	C41-C46	1.525(4)
C21-C26	1.524(4)	C42-C43	1.533(4)
C22-C23	1.526(5)	C43-C44	1.522(5)
C23-C24	1.519(4)	C44-C45	1.522(6)
C24-C25	1.522(6)	C45-C46	1.530(4)

Table S3.2. Cyclohexylammonium trimolybdate hydrate—interatomic distances (**2**).

Mo – O (symm. code)	Distance (esd) Å	Mo – O (symm. code)	Distance (esd) Å
Mo2-O1	2.33(3)	Mo1-O1^iii^	1.97(3)
Mo2-O1^i^	2.30(3)	Mo1-O1^i^	1.97(3)
Mo2-O4	1.73(4)	Mo1-O2	2.21(5)
Mo2-O5	1.73(3)	Mo1-O6	1.73(5)
Mo2-O2^ii^	1.99(3)	Mo1-O3	2.28(4)
Mo2-O3	2.03(2)	Mo1-O7	1.71(5)
(i) -x+2,-y,-z+1; (ii) -x+2,y-1/2,-z+1; (iii) -x+2,y+1/2,-z+1			

Table S3.3. Anilinium trimolybdate dihydrate—interatomic distances (**5**).

Mo – O (symm. code)	Distance (esd) Å	Mo – O (symm. code)	Distance (esd) Å
Mo1-01	1.82(6)	Mo2-01^i^	2.50(12)
Mo1-O2	1.95(9)	Mo2-O3	1.74(5)
Mo1-O3	1.94(8)	Mo2-O5^i^	2.19(7)
Mo1-O4	1.95(8)	Mo2-O6	2.62(12)
Mo1-O5	1.94(9)	Mo2-O11	1.94(9)
Mo1-O6	2.10(8)	Mo2-O12	1.95(8)
Mo3-01	2.36(11)		
Mo3-O3	2.38(8)		
Mo3-O5^ii^	1.96(6)		
Mo3-O6^ii^	2.54(12)		
Mo3-O22	1.94(8)		
Mo3-O23	1.94(8)		
(i) -x+1,y-1/2,-z+1/2		(ii) -x+1,y+1/2,-z+1/2	

4. Kinetic modelling and catalytic results

Kinetic models were developed considering perfectly stirred, isothermal batch reactors and the corresponding material balance according to equation (1):

$$\frac{dC_i}{dt} = r_i \qquad (1)$$

where C_i is the molar concentration of species i (M), t is the reaction time (h) and r_i is the reaction rate of species i. The material balances closed in 100 % for Cy (considering CyOx), Lin (considering mono- and diepoxides, and LinFur) and Ole (considering OleOx).

4.1. *cis*-Cyclooctene reaction

For Cy, the (simplest) kinetic model A considers an irreversible, first-order reaction of Cy (**Scheme S1**) according to equations 2 and 3 with the rate constant k_{Cy} (h^{-1}):

$$\frac{dC_{Cy}}{dt} = -k_{Cy}\, C_{Cy} \qquad (2)$$

$$\frac{dC_{CyO}}{dt} = k_{Cy}\, C_{Cy} \qquad (3)$$

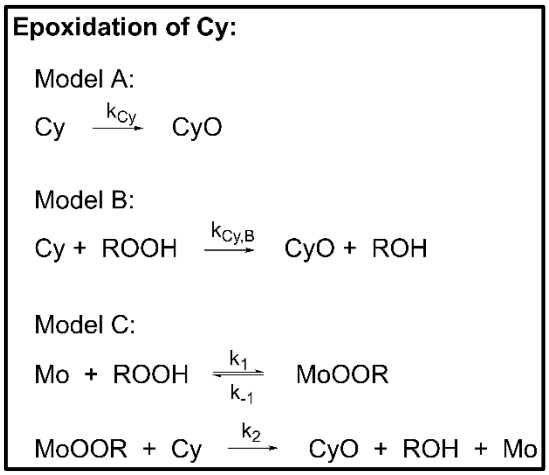

Scheme S4.1. Mechanistic proposal for the reaction of Cy considered for kinetic models A, B and C.

For Cy, the kinetic model B considers the second-order reaction of Cy with TBHP (ROOH; $C_{ROOH,0}$ = initial molar concentration of oxidant, 1.6 M) to CyO plus *tert*-butanol (ROH) (**Scheme S4.1**), according to equations **1**, **4**-**8** with the rate constant $k_{Cy,B}$ ($M^{-1}\,h^{-1}$):

$$\frac{dC_{Cy}}{dt} = -k_{Cy,B}\, C_{Cy} C_{ROOH} \qquad (4)$$

$$\frac{dC_{CyO}}{dt} = k_{Cy,B}\, C_{Cy} C_{ROOH} \qquad (5)$$

$$\frac{dC_{\mathrm{ROOH}}}{dt} = -k_{Cy,B}\ C_{\mathrm{Cy}}C_{\mathrm{ROOH}} \quad (6)$$

$$\frac{dC_{\mathrm{ROH}}}{dt} = k_{Cy,B}\ C_{\mathrm{Cy}}C_{\mathrm{ROH}} \quad (7)$$

For Cy, the kinetic model C considers second-order reactions (**Scheme S4.1**), contemplating the kinetics of formation of active species MoOOR from the interactions between molybdenum ($C_{\mathrm{Mo,0}}$ = initial molar concentration of molybdenum, 0.01 M) and the oxidant ROOH ($C_{\mathrm{ROOH,0}}$ = 1.6 M), according to equations 1, 8-13 with the rate constants k_1 and k_2 ($M^{-1}\ h^{-1}$), and k_{-1} (h^{-1}):

$$\frac{dC_{\mathrm{Cy}}}{dt} = -k_2\ C_{\mathrm{Cy}}C_{\mathrm{MoOOR}} \quad (8)$$

$$\frac{dC_{\mathrm{CyO}}}{dt} = k_2\ C_{\mathrm{Cy}}C_{\mathrm{MoOOR}} \quad (9)$$

$$\frac{dC_{\mathrm{ROOH}}}{dt} = -k_1\ C_{\mathrm{Mo}}C_{\mathrm{ROOH}} + k_{-1}C_{\mathrm{MoOOR}} \quad (10)$$

$$\frac{dC_{\mathrm{ROH}}}{dt} = k_2\ C_{\mathrm{Cy}}C_{\mathrm{MoOOR}} \quad (11)$$

$$\frac{dC_{\mathrm{MoOOR}}}{dt} = k_1\ C_{\mathrm{Mo}}C_{\mathrm{ROOH}} - k_{-1}C_{\mathrm{MoOOR}} - k_2\ C_{\mathrm{Cy}}C_{\mathrm{MoOOR}} \quad (12)$$

$$\frac{dC_{\mathrm{Mo}}}{dt} = -k_1\ C_{\mathrm{Mo}}C_{\mathrm{ROOH}} + k_{-1}C_{\mathrm{MoOOR}} \quad (13)$$

The three kinetic models A–C fitted the experimental results well: F_{obj} in the range 1.9958×10^{-5}-4.7000×10^{-2} for model A; 2.9022×10^{-4}-8.8100×10^{-2} for model B; and 9.5088×10^{-7}-3.9000×10^{-2} for model C. Figures S4.1-S4.3 shows the experimental and calculated curves, indicating relatively good fittings.

Hence, the simpler kinetic model A is reasonable and was used to obtain the results discussed in the main text. The assumptions of model A were considered for the kinetic modelling of the remaining olefins (Ole, Lin).

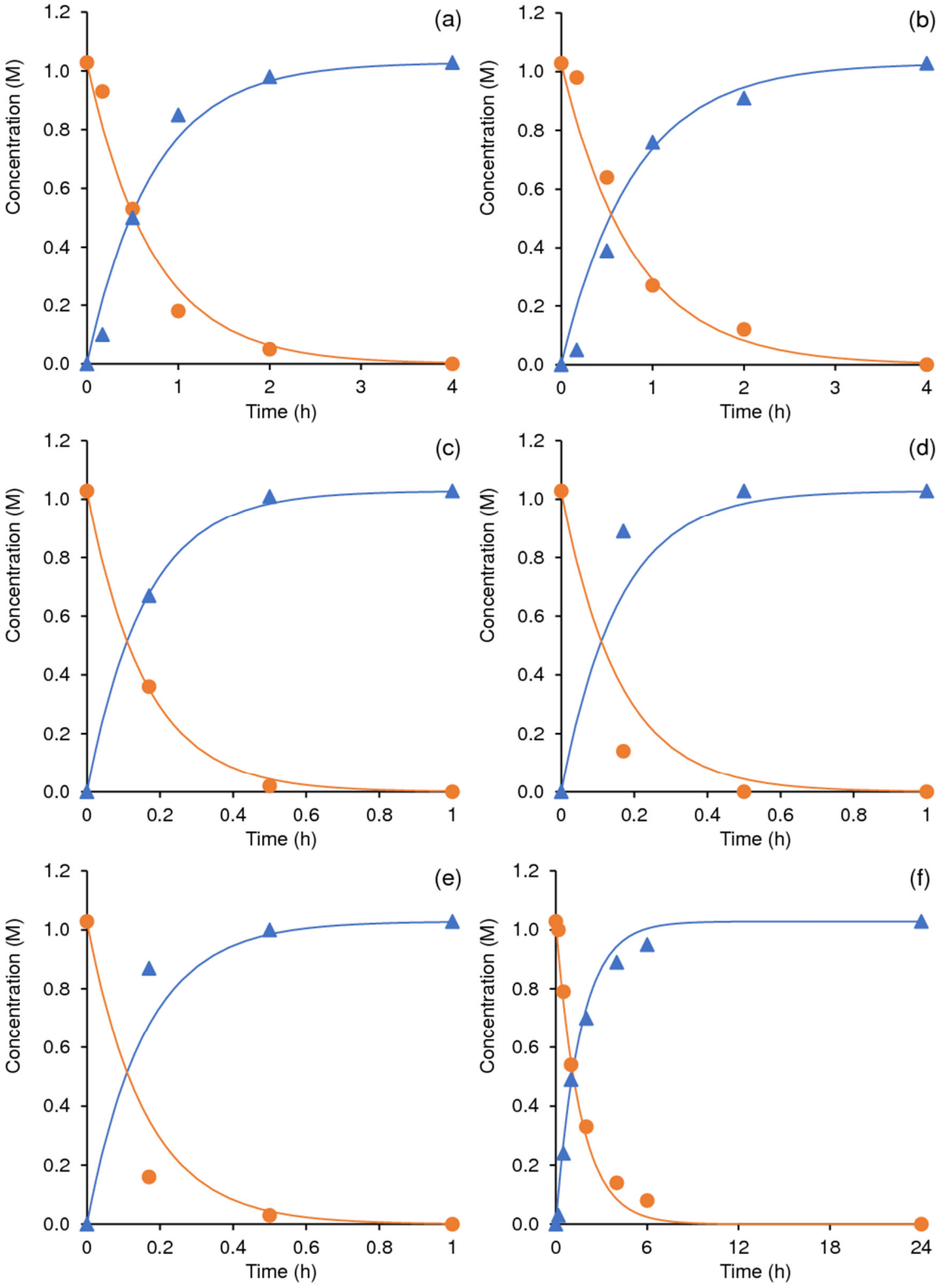

Fig. S4.1. Experimental data (markers) and calculated kinetic curves (lines) for Cy (o) and epoxide CyO (Δ) concentration, based on the model A, for catalysts **1** (a), **2** (b), **3** (c), **4** (d), **5** (e) and **6** (f), at 70 °C.

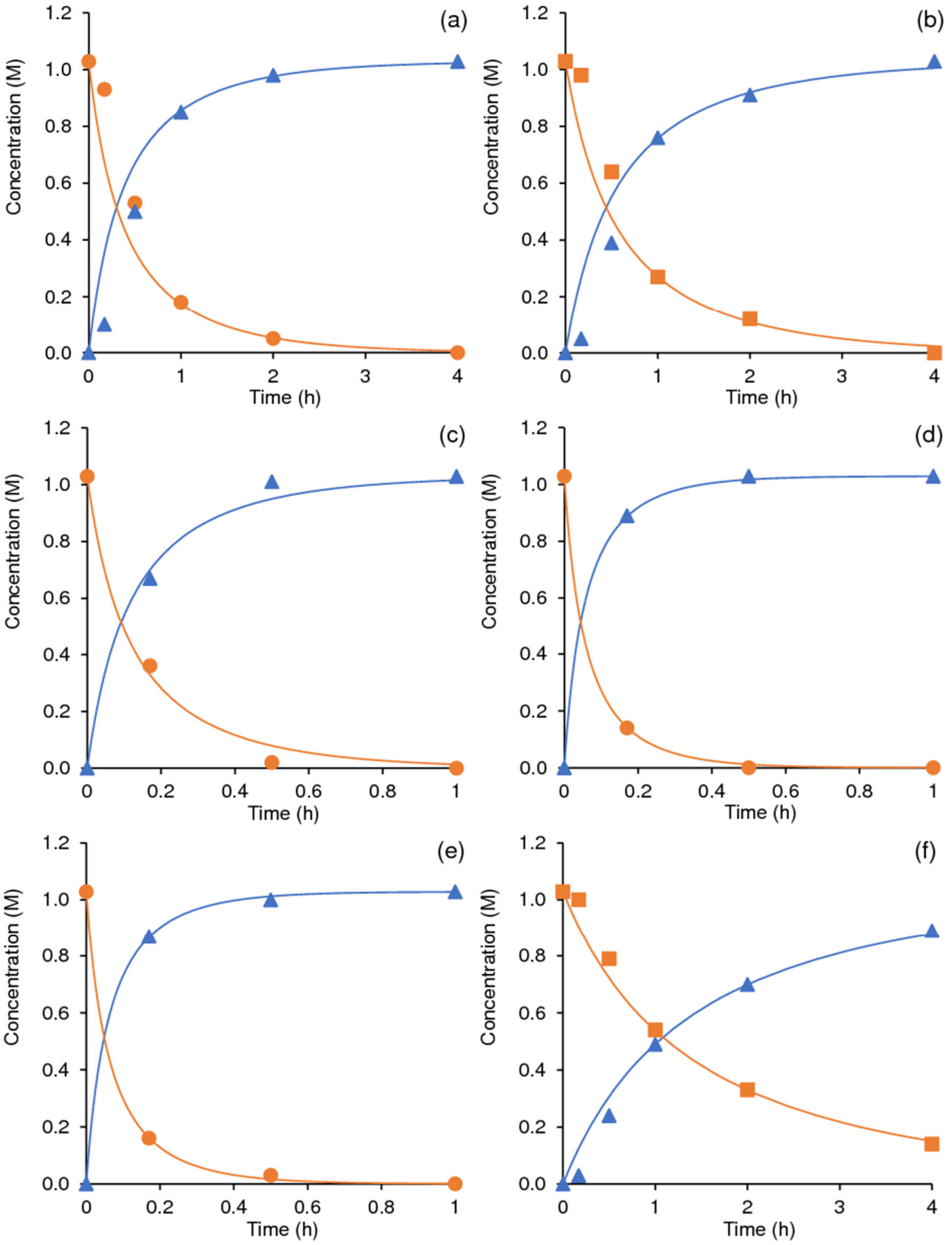

Fig. S4.2. Experimental data (markers) and calculated kinetic curves (lines) for Cy (o) and epoxide CyO (Δ) concentration, based on the model B, for catalysts **1** (a), **2** (b), **3** (c), **4** (d), **5** (e) and **6** (f), at 70 °C.

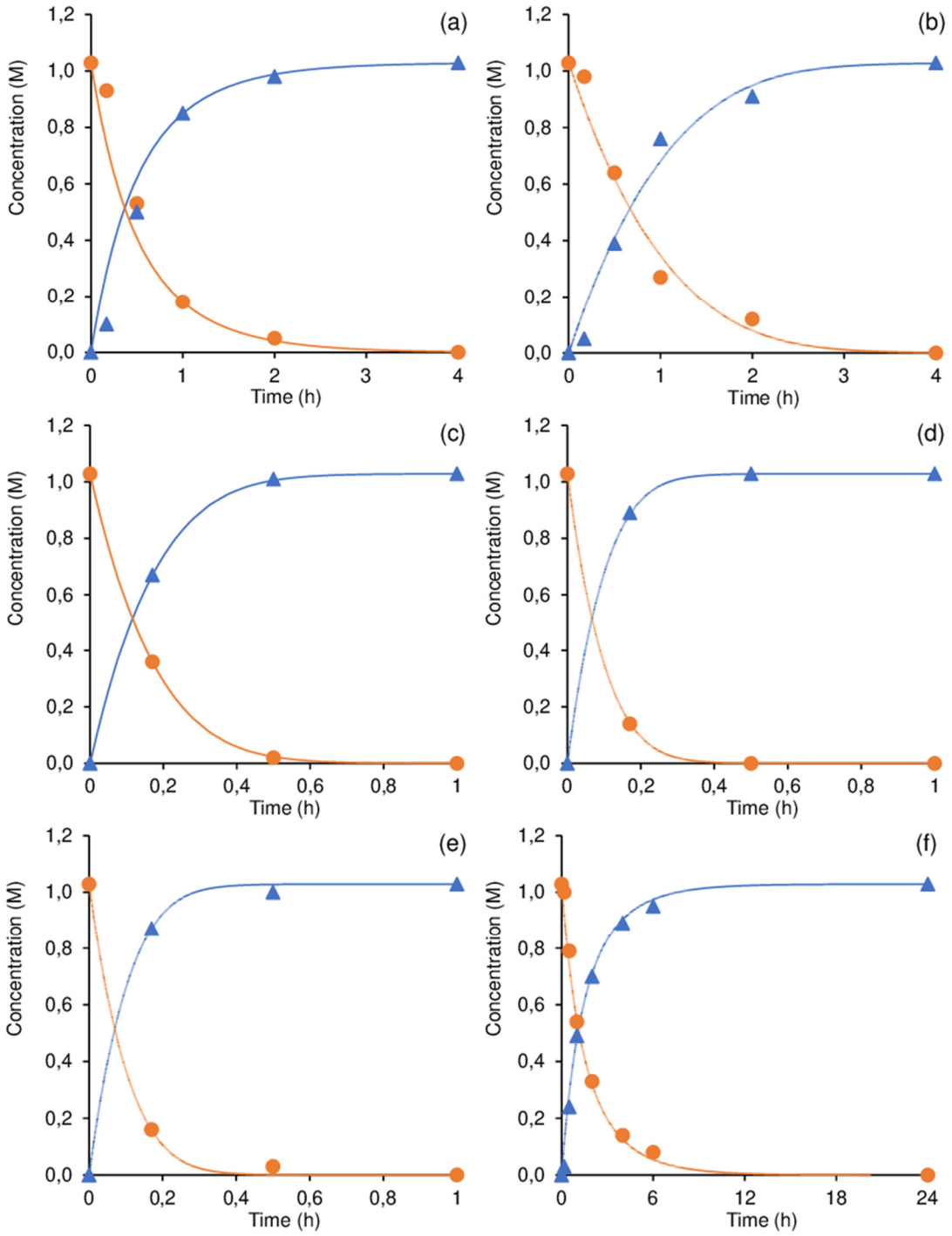

Fig. S4.3. Experimental data (markers) and calculated kinetic curves (lines) for Cy (o) and epoxide CyO (Δ) concentration, based on the model C, for catalysts **1** (a), **2** (b), **3** (c), **4** (d), **5** (e) and **6** (f), at 70 °C.

Table S4.1. Calculated data based on kinetic models A and B, for the Cy reaction, at 70 °C.

Catalyst	Kinetic model	Rate Constant k_{Cy} (model A) or $k_{Cy,B}$ (model B) [a]	F_{obj}
1	A	1.3989	4.0500×10^{-2}
	B	1.1602	8.5700×10^{-2}
2	A	1.0774	4.7000×10^{-2}
	B	0.8841	8.8100×10^{-2}
3	A	6.3279	1.2000×10^{-3}
	B	5.8411	9.2000×10^{-3}
4	A	11.5946	1.9958×10^{-5}
	B	12.1012	2.9022×10^{-4}
5	A	10.9802	1.6000×10^{-3}
	B	11.0396	5.9689×10^{-4}
6	A	0.5565	1.8800×10^{-2}
	B	0.4580	2.3700×10^{-2}

[a] Expressed as h^{-1} and $M^{-1}\ h^{-1}$ for the kinetic models A and B, respectively.

Table S4.2. Calculated data based on kinetic model C, for the Cy reaction, at 70 °C.

Catalyst	Rate Constant (h^{-1})			F_{obj}
	k_1	k_{-1}	k_2	
1	185.1133	0.1329	227.8703	1.4800×10^{-2}
2	114.8381	0.2376	213.0711	3.9000×10^{-2}
3	871.3442	0.1270	984.3523	1.7708×10^{-5}
4	1506.3	0.1000	1700.2	9.5088×10^{-7}
5	1438.3	0.5000	1636.4	2.0000×10^{-3}
6	179.8089	283.1966	153.9463	1.5500×10^{-2}

4.2. Methyl oleate reaction

For methyl oleate (Ole), the kinetic model was based on the mechanism presented in **Scheme S4.2**, considering irreversible, first-order reactions with rate constants k_{Ole} (h^{-1}) (in parallel to model A for Cy), according to equations 1, 14-15:

$$\frac{dC_{\mathrm{Ole}}}{dt} = -k_{Ole}\ C_{\mathrm{Ole}} \qquad (14)$$

$$\frac{dC_{\mathrm{OleOx}}}{dt} = k_{Ole}\ C_{\mathrm{Ole}} \qquad (15)$$

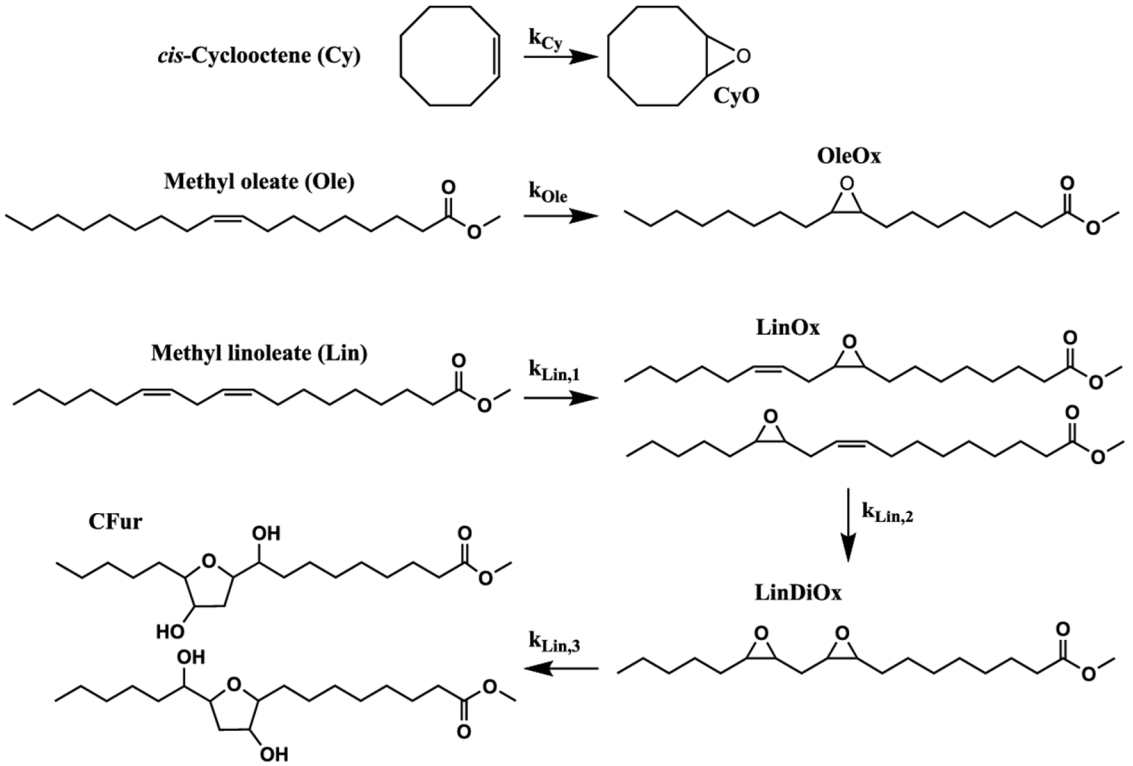

Scheme S4.2. Mechanistic proposal for the reaction of the olefins, considering irreversible, first-order reactions (same as Scheme 1 of the main text, serves as guide).

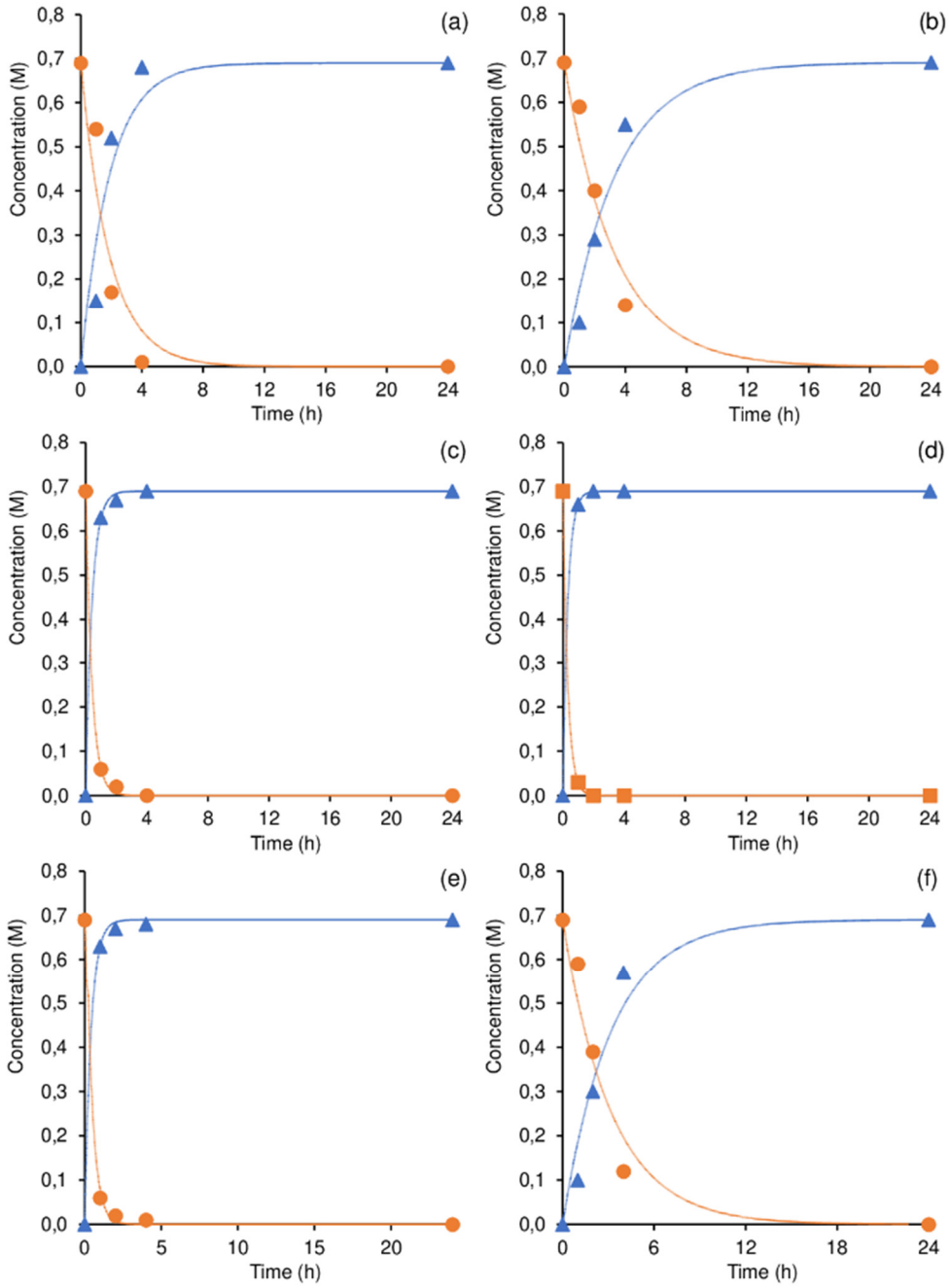

Fig. S4.4. Experimental data (markers) and calculated kinetic curves (lines) for Ole (o) and OleOx (Δ) concentration for catalysts **1** (a), **2** (b), **3** (c), **4** (d), **5** (e) and **6** (f), at 70 °C.

4.3. Methyl linoleate reaction

For methyl linoleate (Lin), the kinetic modelling was based on **Scheme S4.2** and considering irreversible, first-order reactions with rate constants k_j (h^{-1}) (in parallel to model A for Cy), according to equations 16-19:

$$\frac{dC_{\text{Lin}}}{dt} = -k_{Lin,1}\ C_{\text{Lin}} \quad (16)$$

$$\frac{dC_{\text{LinOx}}}{dt} = k_{Lin,1}\ C_{\text{Lin}} - k_{Lin,2}\ C_{\text{LinOx}} \quad (17)$$

$$\frac{dC_{\text{LinDiOx}}}{dt} = k_{Lin,2}\ C_{\text{LinOx}} - k_{Lin,3}\ C_{\text{LinDiOx}} \quad (18)$$

$$\frac{dC_{\text{LinFur}}}{dt} = -k_{Lin,3}\ C_{\text{LinDiOx}} \quad (19)$$

For all substrates, the equation systems were solved by numerical integration in Matlab (version 9.13), using appropriate initial conditions (at $t = 0$), and the solution was refined by minimizing the objective function (F_{obj}) presented in equation (20), giving the values of the kinetic constants (k_i, h^{-1}) by fitting the proposed model to the experimental data.

$$F_{\text{obj}} = \sum_m \left\{ \sum_{n=1}^{n_p} \left[C_{m,n}\big|_{\text{calc}} - C_{m,n}\big|_{\text{exp}} \right]^2 \right\} \quad (20)$$

where $C_{m,n}\big|_{\text{calc}}$ and $C_{m,n}\big|_{\text{exp}}$ are the calculated and experimental concentration values, respectively, at each instant of time n, and for specie m.

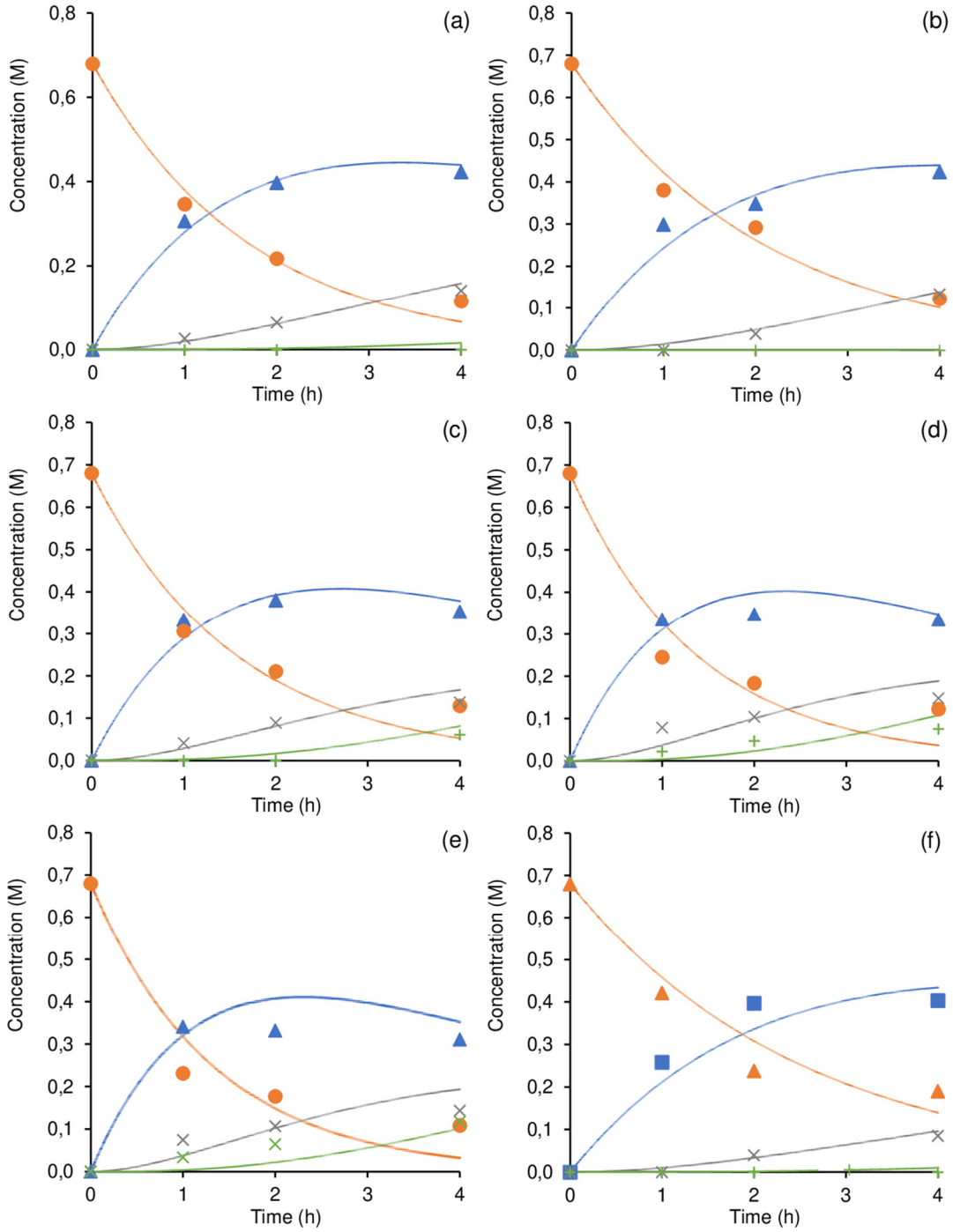

Fig. S4.5. Experimental data (markers) and calculated kinetic curves (lines) for Lin (o), LinOx (Δ), LimDiOx (×) and LinFur (+) concentration for catalysts **1** (a), **2** (b), **3** (c), **4** (d), **5** (e) and **6** (f), at 70 °C.

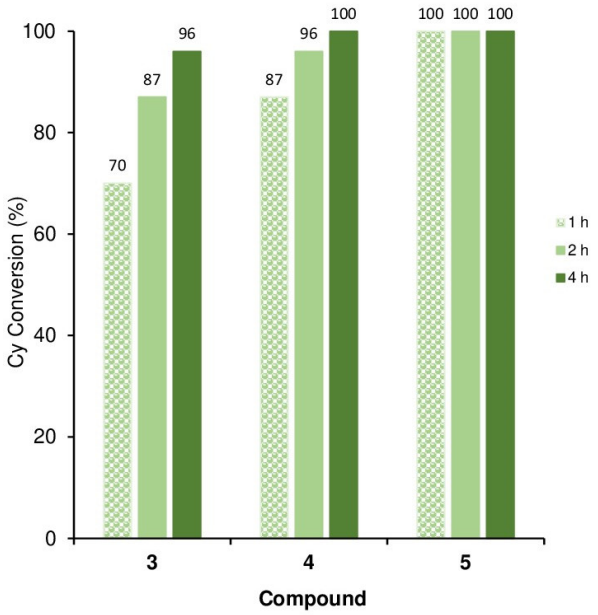

Fig. S4.6. *cis*-Cyclooctene epoxidation with TBHP, in the presence of the IPOM catalysts **3**–**5**, at 55 °C. Epoxide selectivity was always 100 %.

Table S4.3. Comparison of the catalytic results for **3**–**5** to literature data for IPOMs possessing anilinium derivatives as organic components, tested for the Cy/TBHP reaction, at 55 °C.[a]

Catalyst	Dim.[b]	t (h)[c]	Conv. (%)[d]	Ref
3	0-D	1/4	63/96	-
4	1-D	1/4	87/100	-
5	1-D	1	100	-
$(C_8H_{12}N)_2[Mo_3O_{10}]$	1-D	1/6	71/100	[1]
$(C_7H_{10}N)_2[Mo_3O_{10}]$	1-D	1/6	91/100	[1]

[a] Initial molar ratio Mo:olefin:oxidant = 1:100:153. [b] Dim. = Structural dimensionality. [c] t = Reaction time. [d] Conv. = Cy conversion (CyO selectivity was always 100 %).

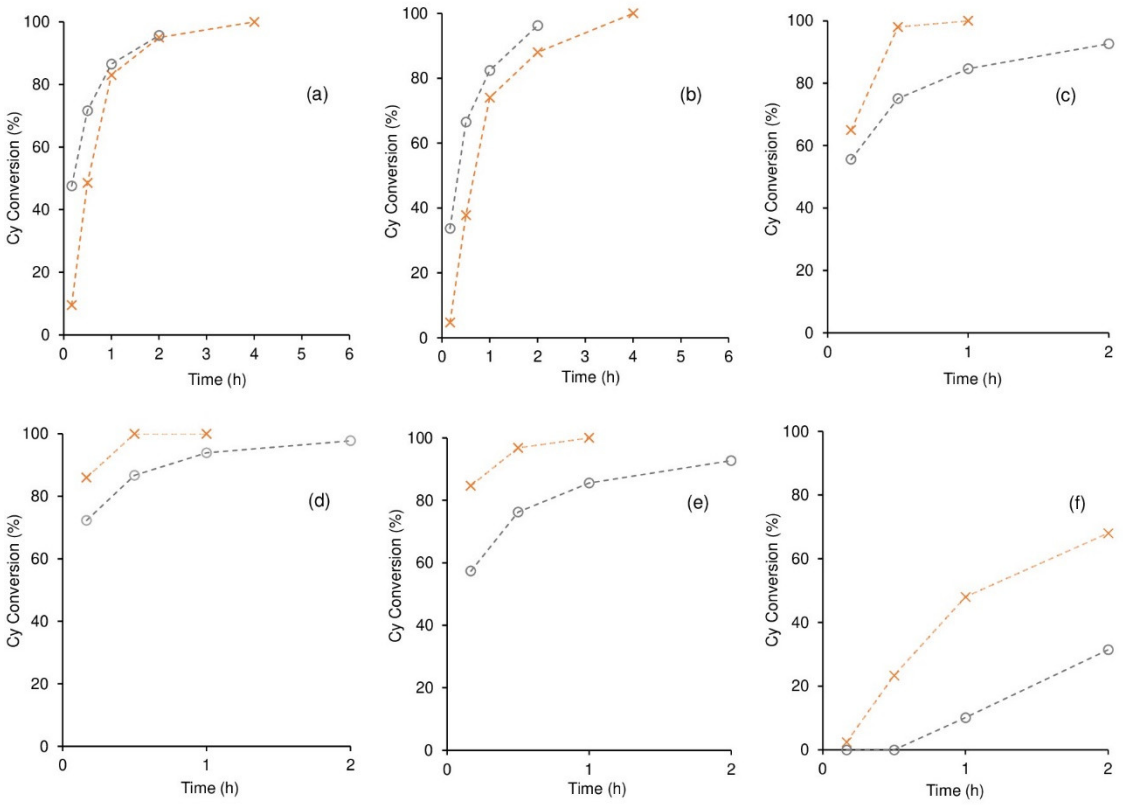

Fig. S4.7. Typical epoxidation catalytic test (with catalyst) (○) and contact tests (×) for *cis*-cyclooctene epoxidation with TBHP, in the presence of the IPOM catalysts **1** (a), **2** (b), **3** (c), **4** (d), **5** (e) and **6** (f), at 70 °C.

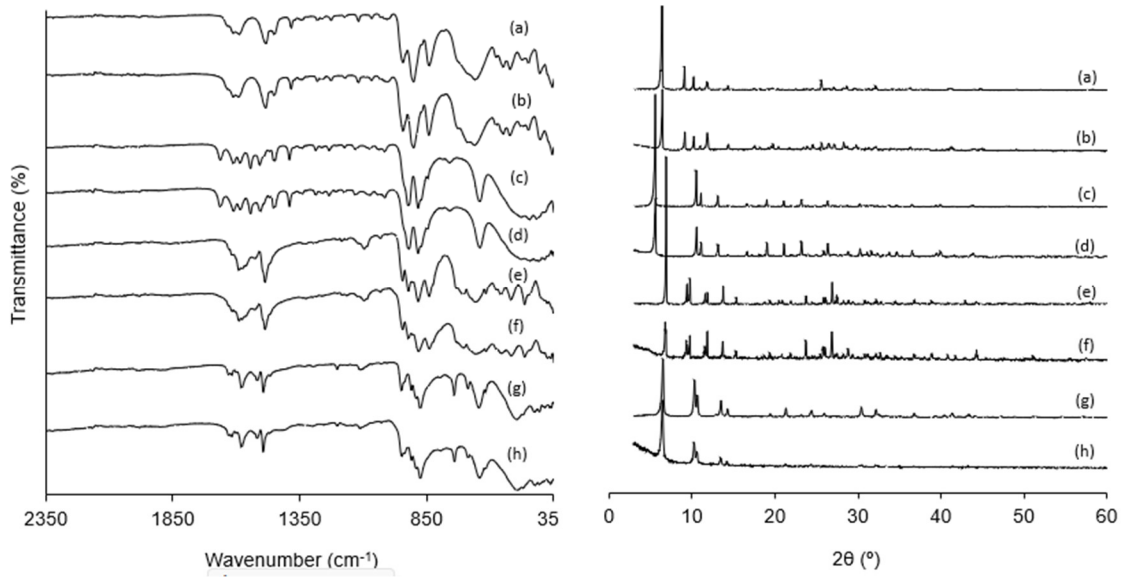

Fig. S4.8. ATR FT-IR spectra (a) and powder XRD patterns (b) of the original and recovered solids: **1** (a), **1**-used (b), **2** (c), **2**-used (d), **3** (e), **3**-used (f), **5** (g), **5**-used (h). The results for **6** were previsouly published, demonstrating its good stability [19]. Compound **4** was structurally similar to **5**.

Routine X-ray powder diffraction (XRPD) data were collected at ambient temperature on a Philips Analytical Empyrean diffractometer equipped with a PIXcel 1D detector, with automatic data acquisition (X'Pert Data Collector software v. 4.2) using monochromatized Cu Kα radiation (λ=1.54178 Å). Intensity data were collected by the step counting method (step 0.02°), in continuous mode, in the 2θ range 5–60°. Attenuated total reflectance (ATR) FT-IR spectra were measured on a Bruker Tensor 27 spectrometer equipped with a Specac Golden Gate Mk II ATR accessory having a diamond top plate and KRS-5 focusing lenses (resolution 4 cm^{-1}, 128 scans).

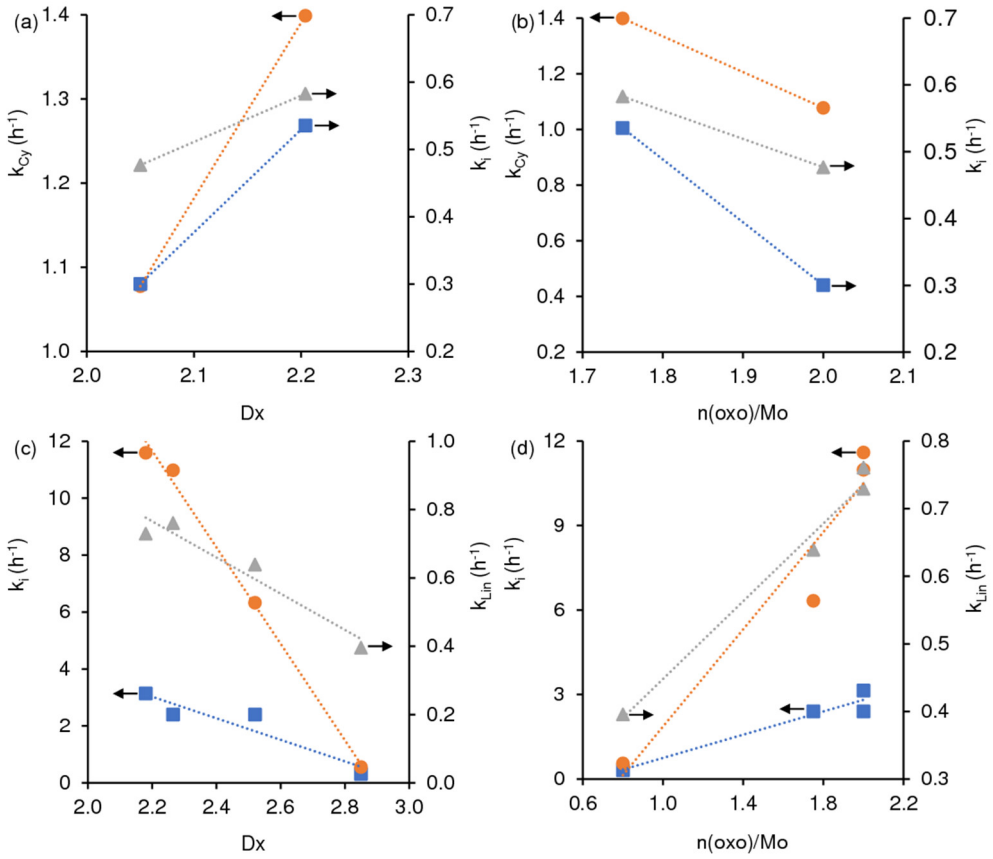

Fig. S4.9. Kinetic constants as a function of density Dx (left) and n(oxo)/Mo ratio (right), for the Cy6N (**a**, **b**) and Anil (**c**, **d**) families of IPOM catalysts with different substrates (Cy (circles), Ole (squares) and Lin (triangles); the dotted lines are trendlines).

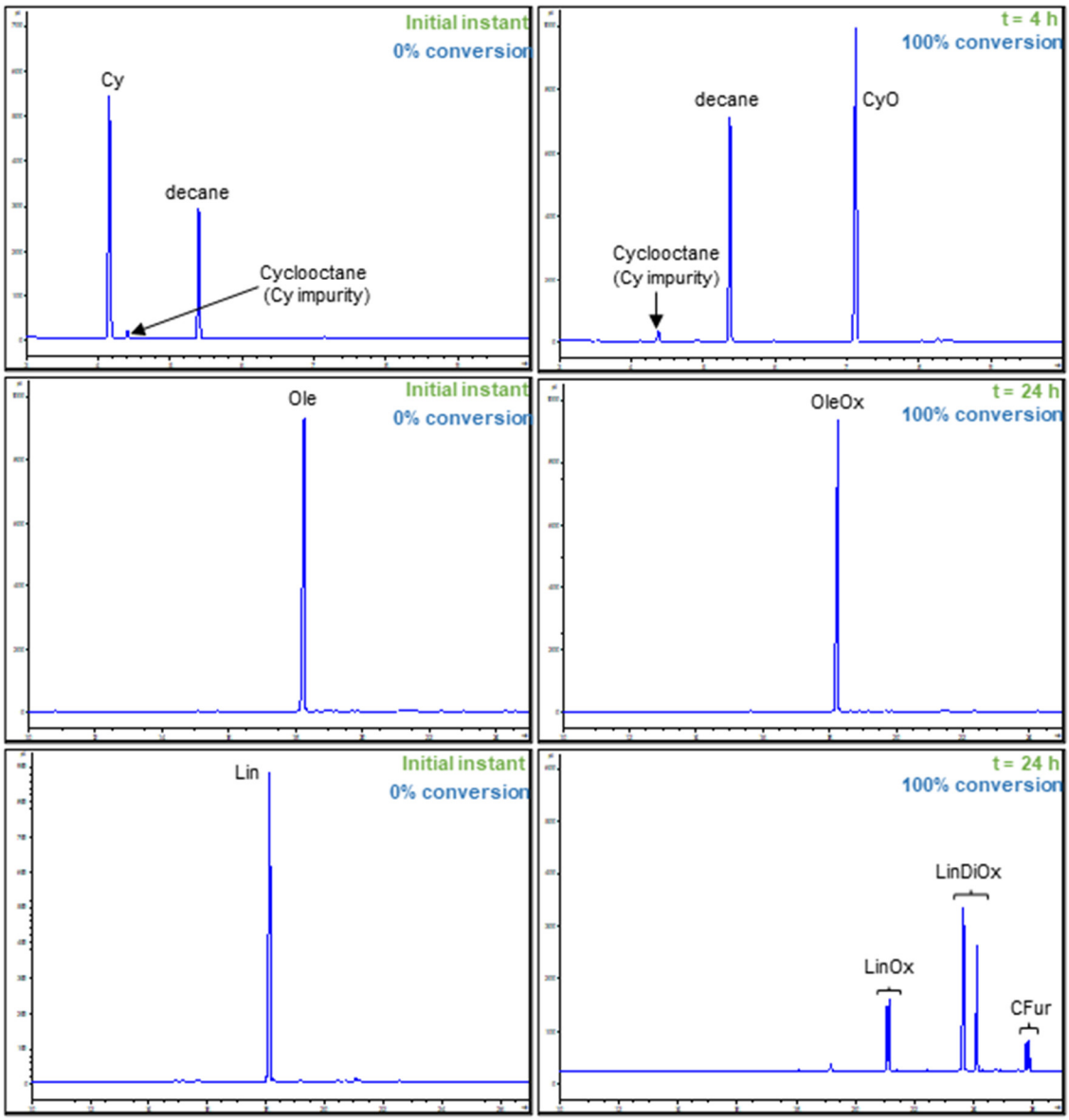

Fig. S4.10. Examples of GC chromatograms for the reaction of olefins (a) Cy, (b) Ole, (c) Lin, in the presence of **2**/TBHP/TFT at 70 ºC.